RESEARCH ARTICLE

INTERNATIONAL RESEARCH JOURNAL OF MULTIDISCIPLINARY TECHNOVATION

Asian Research Association

DOI: 10.54392/irjmt26417

Development of Eco-Friendly Prosopis Juliflora Fiber-Reinforced Epoxy Composites with Mg $(OH)_2$ and TiO_2 Nanofillers for Improved Mechanical and Fire-Retardant Properties

N. Shalom [a], R. Haridass [a], Pravin Kulurkar [b], S. Mayakannan [c, d, *]

[a] Department of Mechanical Engineering, Karpagam College of Engineering, Coimbatore, Tamil Nadu, India
[b] Department of Computer Science & Engineering, JD College of Engineering & Management, Nagpur, Maharashtra-441501, India.
[c] School of Engineering, Saveetha Institute of Medical and Technical Sciences, Saveetha university, Chennai, Tamil Nadu, India
[d] Department of Mechanical Engineering, Rathinam Technical Campus, Coimbatore, Tamil Nadu, India
* Corresponding Author Email: kannanarchieves@gmail.com

DOI: https://doi.org/10.54392/irjmt26417

Received: 11-11-2025; Revised: 26-06-2026; Accepted: 08-07-2026; Published: 25-07-2026

Abstract: Natural fiber–reinforced polymer composites are emerging as viable alternatives to synthetic materials, especially in heat- and fire-resistant applications, due to increasing environmental consciousness and the need for biodegradable options. Eco-friendly epoxy composites reinforced with 20 wt. % alkali-treated *Prosopis juliflora* fibers and $Mg(OH)_2/TiO_2$ nanofillers (2–6 wt.%) were fabricated using the hand lay-up method to enhance mechanical, thermal, fire-retardant, and moisture resistance properties. XRD analysis confirmed increased crystallinity after alkali treatment (71.86% to 72.98%), indicating removal of amorphous constituents, while FTIR spectra validated improved interfacial compatibility. SEM micrographs revealed enhanced fiber–matrix adhesion and minimal void formation at 4 wt. % filler loading, whereas 6 wt. % caused nanoparticle agglomeration. The optimum composition exhibited a tensile strength of 64.60 MPa (30.29% improvement) and flexural strength of 21.89 MPa (54.86% improvement) compared to the control (49.58 MPa). Impact strength increased to 21.67 kJ m^{-2} (71.2% enhancement). Cone calorimetry demonstrated a reduction in peak heat release rate from 420 kW m^{-2} to 402 kW m^{-2} (4.3% reduction), while the burning rate decreased below 35 mm min^{-1} for nanoparticle-filled composites. TGA results showed improved onset degradation temperature up to 348.6 °C and increased char residue to 11.5%. Water absorption decreased by up to 8.18% due to the barrier effect of nanofillers. The synergistic incorporation of $Mg(OH)_2$ and TiO_2 significantly improved multifunctional performance, making the composites suitable for lightweight structural and fire-resistant applications.

Keywords: Prosopis Juliflora Fibers, Titanium Dioxide, XRD Analysis, FTIR Analysis, Mechanical Properties.

1. Introduction

The predominant thermosetting resins are polymer compounds such as vinyl ester, epoxy, and polyester. Thermoset-based natural fiber composites exhibit exceptional creep and solvent resistance. Prosopis juliflora, also known as Neltuma juliflora, was selected due to its low density (~1.48 g/cm³), high cellulose content, acceptable tensile strength, biodegradability, and wide availability as an invasive biomass resource in tropical regions. Its utilization supports environmental management by converting an invasive species into a value-added engineering material. Previous studies have demonstrated its favorable mechanical behavior, surface modifiability through alkali treatment, and compatibility with thermoset matrices [1]. These characteristics make Prosopis juliflora a promising reinforcement candidate for sustainable composite development. Prosopis juliflora (PJ) fibers and palm kernel seed powder were embedded in epoxy by compression moulding. Ageing tests showed that 30 wt% silane-treated PJ fibers improved mechanical strength, while palm seed fillers enhanced hardness. The composites exhibited good water resistance, making them suitable for automobile and light roofing applications [2]. Prosopis juliflora fiber-reinforced polylactic acid composites were enhanced with ZnO nanofillers. The S5 sample showed a tensile strength of 67.29 MPa, a flexural strength of 64.27 MPa, a compressive strength of 56.79 MPa, and an impact energy of 34 J. TGA indicated a degradation temperature of 312–342 °C, while SEM confirmed improved fracture behavior [3]. Silane-treated Prosopis juliflora fiber epoxy composites with Syzygium cumini

filler (SCF) were studied. The ST/SCF3 composites achieved the best results, with an impact strength of 27.83 kJ/m², a tensile strength of 118.65 MPa, and a hardness of 91.63 HV. Wear resistance, friction reduction, and thermal stability were significantly improved in silane-treated composites [4]. Epoxy composites with Prosopis juliflora (PJ), Abutilon indicum, and Tapsi fibers (20 wt%) were fabricated by the hand lay-up technique. Mechanical and wear tests revealed that PJ-based composites showed superior flexural, wear, tensile, and impact resistance compared to the other fibers. SEM confirmed better bonding and a reduced material removal rate [5]. Hybrid epoxy composites reinforced with Prosopis juliflora fibers (PJF), E-glass, and carbon fabrics were fabricated by the hand lay-up technique. The stacking sequence influenced physical, mechanical, and morphological properties. Results showed that hybridization with glass and carbon improved overall performance, making the composites suitable for structural engineering applications [6]. Red Sage Fiber (RSF) and Prosopis juliflora fiber (PJF) were extracted, NaOH-treated, and incorporated into PLA composites. Treated PJFs showed higher tensile strength (149.9–182.3 MPa) and reduced water absorption, while RSF enhanced flexural strength. PLA composites with PJFs up to 15 wt% demonstrated better tensile strength and hydrophobicity than neat PLA [7]. Prosopis juliflora fibers were utilized as reinforcement in gypsum plaster to improve brittleness. Fibers treated with NaOH, $KMnO_4$, and distilled water enhanced fiber–matrix interaction. Results showed improved flexural strength, toughness, and a shift from brittle to ductile failure, making the plaster more sustainable for construction use [8].

Epoxy-based hybrid composites reinforced with Calotropis gigantea (CG) and Prosopis juliflora (PJ) fibers were fabricated. The best combination (20 wt% Calotropis, 20 wt% PJ, 6% NaOH, 100 °C, 14 MPa) showed superior tensile, flexural, and impact strengths [9]. Prosopis juliflora and glass fiber hybrid composites were fabricated at varying weight ratios. Among four samples, the 12% PJ + 28% glass sample showed the highest impact energy (2.6 J), while water absorption varied with fiber proportions. Improved impact strength and water resistance made the composites suitable for automotive and structural applications [10]. Pineapple/sisal hybrid epoxy composites were reinforced with 3–5 wt% TiO_2. Mechanical properties improved, with tensile (+11.6%), flexural (+8.8%), and impact (+8.3%) strengths maximized at 5 wt%. Tribological studies confirmed reduced wear and better friction stability [11]. Calotropis gigantea fiber/PP composites (40 wt%) showed the best mechanical strength (225% higher impact and 54% higher tensile strength than virgin PP). Silane treatment enhanced adhesion and thermal stability. $Mg(OH)_2$ addition reduced the combustion rate [12]. Kenaf fiber/PET/epoxy composites with $Mg(OH)_2$ showed the lowest burning rate at 35% KF (14.55 mm/min). Maximum tensile strength was achieved at 50% KF. SEM confirmed reduced surface defects at the optimal fiber content [13]. Reactive magnesia reinforced with hollow natural fibers (sisal) enhanced compressive strength (20.9 → 39.3 MPa). Fibers improved CO_2 diffusion, boosting carbonation depth and material strength. Minimal fiber degradation occurred in the $Mg(OH)_2$ matrix [14]. Hemp fiber/epoxy composites with $Mg(OH)_2$ and $Al(OH)_3$ improved thermal stability and flame retardancy. LOI increased up to 25.3%, with the lowest burning rate of 11.6 mm/min. A slight reduction in mechanical strength was observed [15]. The incorporation of 6 wt.% hydrophobic TiO_2 nanoparticles significantly enhanced the mechanical properties of fabricated polypropylene/kenaf fiber composites. Compared with the neat polypropylene matrix, the optimized composite exhibited 62% higher tensile strength, 47% higher flexural strength, and 70% higher impact strength due to improved fiber–matrix interfacial bonding [16]. X-ray diffraction (XRD) was used to characterize the crystalline structure of the magnesium hydroxide Mg $(OH)_2$ particles used for coating kenaf fibers. The XRD analysis confirmed the crystalline nature of the MH coating, validating its successful incorporation for improving the fiber–matrix interfacial bonding in polypropylene composites [17].

Although several studies have reported Prosopis juliflora fiber composites reinforced with single nanofillers such as ZnO or TiO_2, limited research has investigated the synergistic interaction between Mg $(OH)_2$ and TiO_2 in a single epoxy-based natural fiber system. Furthermore, the combined influence of dual hydroxide-based flame retardants on mechanical, thermal, fire-retardant, and moisture resistance properties has not been systematically correlated with microstructural evidence. Therefore, the present study addresses this gap by evaluating the hybrid reinforcement effect of $Mg(OH)_2$ and TiO_2 nanoparticles at optimized loadings and establishing structure–property relationships through SEM, FTIR, XRD, TGA, and cone calorimetry analyses.

2. Materials and Methodology

2.1 Materials

The bidirectional Prosopis juliflora fiber (density: 1.48 g/cm³) was obtained from Gogreen Enterprises, Chennai, Tamil Nadu, India. A diglycidyl ether of bisphenol-A (DGEBA)-based epoxy resin (LY 556) with a viscosity of 10–12 Pa·s at 25 °C and a density of 1.31 g/cm³ was procured from Kovai Cheenu Enterprises, Coimbatore, Tamil Nadu, India. The hardener used was triethylenetetramine (TETA), mixed in a 10:1 resin-to-hardener ratio as recommended by the manufacturer. Mg $(OH)_2$ nanoparticles with a density of 2.36 g/cm³ and TiO_2 with a density of 4.23 g/cm³ were acquired from Matrics Enterprises, Nagercoil, Tamil Nadu, India. In this

research, nanofillers such as Mg $(OH)_2$ and TiO_2 were incorporated for the following scientific reasons. The integration of magnesium hydroxide (Mg $(OH)_2$) into polymers, especially epoxy-based composites, significantly improves their fire resistance [18]. The principal process is endothermic decomposition, wherein Mg $(OH)_2$ absorbs considerable heat throughout its disintegration, occurring at temperatures roughly between 330 and 340 °C. The production of water vapor in this reaction reduces the concentration of combustible gases and hinders flame propagation, as demonstrated in Eq. 1. The thermally stable barrier layer of magnesium oxide (MgO) improves performance by augmenting insulation and facilitating a protective char over the materials. Moreover, magnesium hydroxide (Mg $(OH)_2$) is free of halogens, presents no safety hazards, and is appropriate for the fabrication of environmentally sustainable composites.

$$2\mathrm{Mg}\,(\mathrm{OH})_2 \cdot\!\rightarrow\cdot \mathrm{MgO} + \cdot\, 3\mathrm{H_2O} \quad (1)$$

The incorporation of nano-titanium dioxide (TiO_2) significantly enhances the mechanical and thermal resilience of hybrid composites [19]. The improved tensile, flexural, and impact strengths result from the robust interfacial bond established between the Prosopis juliflora fibers and the epoxy matrix, facilitated by the nano-TiO_2 particles and attributed to their uniform distribution and extensive surface area. The exceptional thermal stability of TiO_2, with a breakdown temperature above 750 °C, facilitates the preservation of matrix integrity and enhances overall heat resistance. Besides restricting the transfer of heat and oxygen, the TiO_2 nanoparticles integrated inside the composite function as a barrier that reduces the diffusion of combustible gases during combustion. The specified combinations enhanced the strength of the nanocomposites and reduced their flammability under high temperatures.

2.2 Surface Modification of Prosopis Juliflora Fibers

To achieve surface sterilization, the Prosopis juliflora fibers were immersed in 5 wt% sodium hydroxide for four hours. The fibers were meticulously cleaned with pure deionized water three or four times to remove any residual sodium hydroxide solution adhering to their surfaces. Subsequently, they were permitted to air-dry for 24 hours.

2.3 Composite Fabrication

The chosen nanoparticles were combined with epoxy resin using magnetic stirring to produce the hybrid composite. The epoxy resin and hardener were mixed as per the supplier's guidelines, and to ensure homogeneous dispersion, the nanomaterials were incrementally integrated into the resin while the mixture was agitated at 600 rpm for 40 minutes.

The Prosopis juliflora fiber was evenly coated with the nanoparticle-epoxy composite using a hand lay-up roller. The laminate fabrication procedure followed the methodology reported in a previous study [20]. A mild steel mold was employed to impregnate the Prosopis juliflora fibers. Screws, nuts, and bolts were employed on the mold, and the curing process was sustained at ambient temperature for 24 hours. Release wax was applied to the mold surfaces prior to casting to simplify demolding. Figure 1 depicts the composite fabrication process.

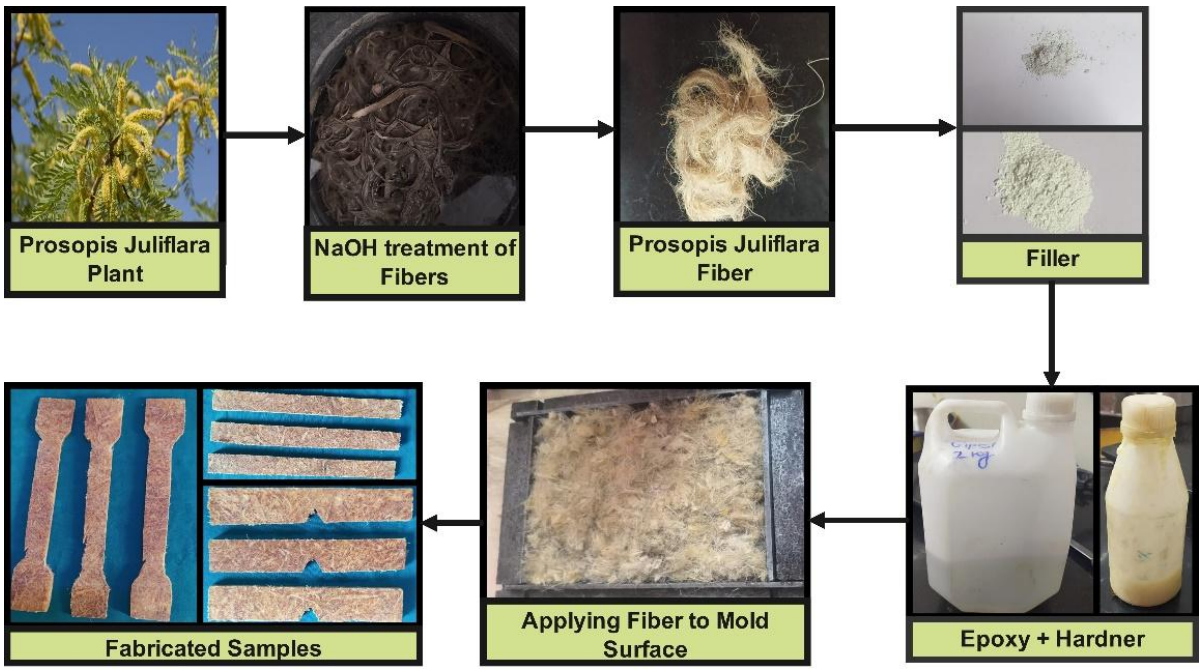

Figure 1. Fabrication process of the composite specimen.

Table 1. Composition of Prosopis juliflora fiber/TiO_2/(Mg $(OH)_2$)-based hybrid composites

Sl. No	Specimen code	Prosopis juliflora fiber (wt.%)	(Mg $(OH)_2$) (wt.%)	TiO_2 (wt.%)	Epoxy resin (wt.%)
1	S1	20	0	0	80
2	S2	20	2	0	78
3	S3	20	4	0	76
4	S4	20	6	0	74
5	S5	20	0	2	78
6	S6	20	0	4	76
7	S7	20	0	6	74
8	S8	20	1	3	76
9	S9	20	3	1	76
10	S10	20	2	2	76

The concluding phase of post-curing entailed a 60-minute exposure in a hot-air oven. The laminates exhibited a thickness of 3 mm and fiber loading of 20 wt%. A fiber loading of 20 wt.% was selected for improved mechanical performance and adequate resin wetting at this fraction without inducing excessive void formation or fiber agglomeration. Preliminary trials indicated uniform dispersion and optimal handling characteristics at this loading.

Table 1 illustrates that the fillers employed in this study were TiO_2 and $Mg(OH)_2$ nanomaterials with different weight percentages. An effective range of 2–6 wt.% was selected for enhancing thermal and mechanical performance [21]. To examine potential synergistic effects, composites were prepared with varying quantities of TiO_2 and $Mg(OH)_2$, along with hybrid combinations (2–4 wt.% of each). The laminate underwent a two-stage curing process: initially at ambient temperature for 1 day, followed by a post-curing phase at 60 °C for 60 minutes. This facilitated the slow hardening of the resin and enhanced crosslinking, thereby reducing internal stresses and ensuring consistency.

2.4 Characterization

2.4.1 X-Ray Diffraction (XRD)

XRD analysis was conducted using a Bruker D8 Advance diffractometer (Bruker AXS, Germany) for both untreated and hydroxide-treated Prosopis juliflora fibers to obtain the crystallinity index of the fibers. The experiments were performed using Cu-Kα radiation with a wavelength of 1.5406 Å at 40 kV and 30 mA. Scans were conducted over a 2θ range of 10° to 80°.

2.4.2 Fourier Transform Infrared Spectroscopy (FTIR)

FTIR spectra were recorded using a Shimadzu IRTracer-100 spectrometer (Shimadzu Corporation, Japan). The untreated and chemically treated Prosopis juliflora fibers were analyzed using a Shimadzu FTIR spectrometer. The spectra were obtained within the 4000–400 cm^{-1} range at a resolution of 4 cm^{-1}. This analysis facilitated the identification and characterization of functional groups in Prosopis juliflora fiber, the epoxy matrix, and the flame-retardant additives (Mg $(OH)_2$ and TiO_2).

2.4.3 Mechanical Characterization

Tensile tests were performed on specimens measuring 250 mm × 25 mm × 3 mm, adhering to the requirements established by ASTM D3039. An Instron universal testing machine (Instron 3369, Instron, USA) with a capacity of 100 kN was utilized, operating at a cross-head speed of 2 mm/min. A standardized testing protocol was employed to perform the flexural test in accordance with ASTM D790. The cross-head speed was 2 mm/min. In accordance with ASTM D256 standards, all specimens were evaluated using an Izod impact apparatus measuring 64 × 12.7 × 3 mm. The data are more dependable, as each test was conducted three times and the mean results were considered.

2.4.4 Flammability Testing

The materials underwent horizontal burning tests in compliance with UL-94 criteria. The combustion durations and intensities of each composite were calculated. The fire performance of the composites was evaluated using a cone calorimeter. Cone calorimeter testing was conducted using a Fire Testing Technology (FTT) cone calorimeter (UK). ASTM E1354 was followed for fire-retardant evaluation. All composite specimens were exposed to an intensity of 60 kW/m^2 for assessment. This experiment quantified flame parameters such as ignition duration, efficient burning rate (EBR), cumulative smoke production rate (CSPR), rate of heat release, highest rate of heat release, and the generation of CO and CO_2.

2.4.5 Thermal Degradation

Thermogravimetric analysis (TGA) was carried out using a PerkinElmer TGA 4000 system (PerkinElmer, USA). All composites were evaluated for thermal endurance using a thermal spectrometer under nitrogen flow at 20 mL/min, while the materials were

subjected to a heating rate of 20 °C/min. Specimens weighing 10–15 mg were utilized consistently throughout the investigation. The weight loss of nanocomposite materials, both with and without nanoparticles, was observed during the experiment in relation to temperature. The laminated composite was subjected to a temperature range of 20–500 °C to obtain the results.

2.4.6 Water Absorption

According to ASTM D570-98, the specimens were analyzed by submerging the composite specimens for 24 to 192 hours and recording the weight variations of the hybrids at 24-hour intervals. To determine the percentage of water absorbed by the epoxy/Prosopis juliflora/($Mg(OH)_2$)/TiO_2 specimens, the following formula was employed:

$$\text{Water absorption} = \frac{W_2 - W_1}{W1} \times 100 \quad (2)$$

2.4.7 FESEM

The specimens were analyzed using a Zeiss FESEM (Carl Zeiss, Germany) model Gemini at the Bannari Amman Institute of Technology in Sathyamangalam, Tamil Nadu, India, focusing on their external and internal surfaces. Initially, a flat aluminum stub was affixed with carbon to secure all specimens, comprising fractured surfaces of the epoxy, the chemically treated fibers/PJF/($Mg(OH)_2$)/TiO_2 composite, and untreated Prosopis juliflora fibers. A thin layer of gold was deposited onto the mounted samples to facilitate electrical measurements without inducing charge during the scan.

3. Results and Discussion

3.1 XRD Analysis

Figure 2 shows the XRD of both untreated and treated Prosopis juliflora fibers, employed to examine their structural and crystallographic characteristics. The XRD pattern of Prosopis juliflora fiber exhibited a characteristic crystalline peak at approximately 2θ ≈ 22° corresponding to the (002) plane of cellulose I, while the amorphous region was observed around 2θ ≈ 18°. Following alkali treatment, the intensity of the (002) peak increased, indicating improved crystallinity due to the removal of amorphous hemicellulose and lignin components.

The crystallinity index (CI) was calculated using the Segal empirical method:

$$CI\ (\%) = [(I002 - Iam) / I002] \times 100 \quad (3)$$

Where *I002* represents the maximum intensity of the crystalline peak at 2θ ≈ 22° and *Iam* corresponds to the minimum intensity at 2θ ≈ 18°.

The crystallinity indices of Prosopis juliflora fiber increased following hydroxide treatment, as evidenced in Figure 2 and Table 2.

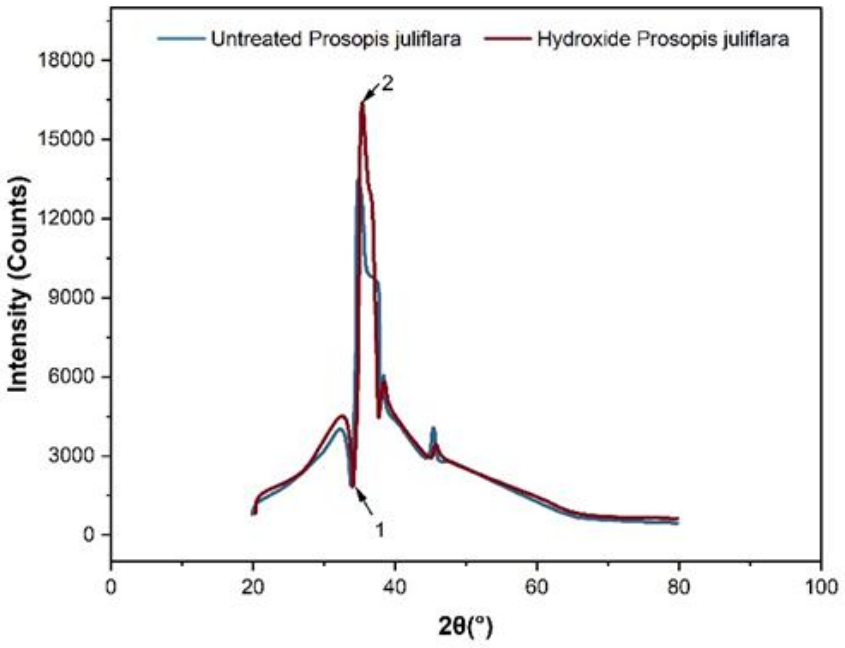

Figure 2. X-ray diffraction analysis of hydroxide-treated and raw Prosopis juliflora fiber.

Table 2. Crystallinity of hydroxide-treated and untreated hybrid composites

S. No	Fiber	I_1	I_2	Crystalline index (%)
1	Untreated Fiber	4125	14850	71.86
2	Hydroxide Treated Fiber	4290	16920	72.98

Hydroxide-treated Prosopis juliflora fiber has crystallinity indices that are 1.12% greater than those of untreated fiber. The crystallinity index was highest for the treated fiber. The remarkable crystallinity indices resulted from the efficient elimination of contaminants and hemicellulose, a phenomenon noted in several cellulose fibers, including Prosopis juliflora and alfa fiber, subjected to alkaline treatment. The crystallinity indices of Prosopis juliflora fiber were elevated when hydroxide-treated fiber was employed [22]. The elimination of amorphous substances during chemical processing improves cellulose packing and mitigates stress, perhaps leading to enhanced crystallinity indices in the processed fibers. The crystallinity indices of both untreated and hydroxide-treated Prosopis juliflora fibers are presented in Table 2. An improved cellulose matrix, evidenced by increased CI, promotes adhesion between cellulose and epoxy. The mechanical performance, thermal characteristics, and stiffness of fiber-reinforced composites improve with an increase in the crystallinity of the polymer chain. Overall, the treatment enhances the material's crystallinity, resulting in superior composite properties demonstrated in subsequent mechanical tests. In previous studies, XRD analysis was performed on both untreated and alkali-treated Prosopis juliflora fiber-reinforced composites to evaluate their crystalline structure. The results revealed enhanced crystallinity in the treated composites, indicating improved fiber–matrix interaction and contributing to better thermal and mechanical performance [23].

3.2 FTIR Analysis

The FTIR characteristics of hydroxide-treated and untreated Prosopis juliflora fibers incorporating (Mg $(OH)_2$) and TiO_2 nanofillers are illustrated in Figures 3 and 4.

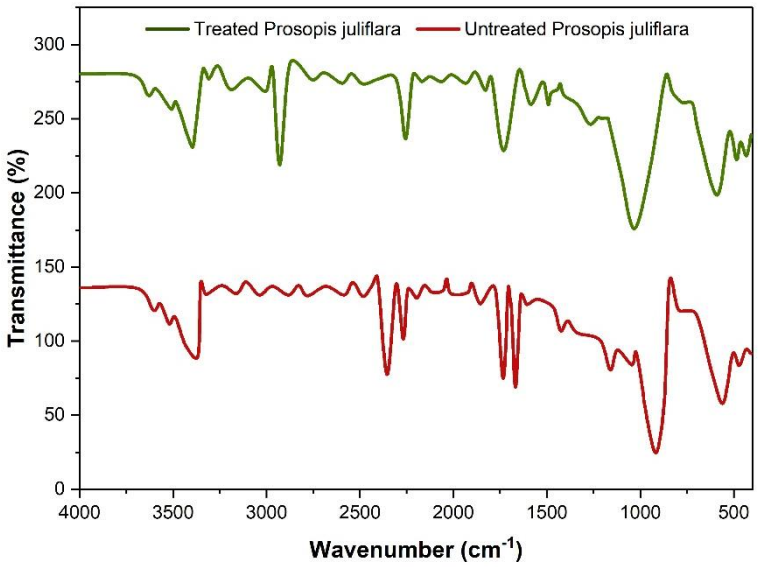

Figure 3. FTIR analysis of hydroxide-treated and untreated Prosopis juliflora fiber-based composites.

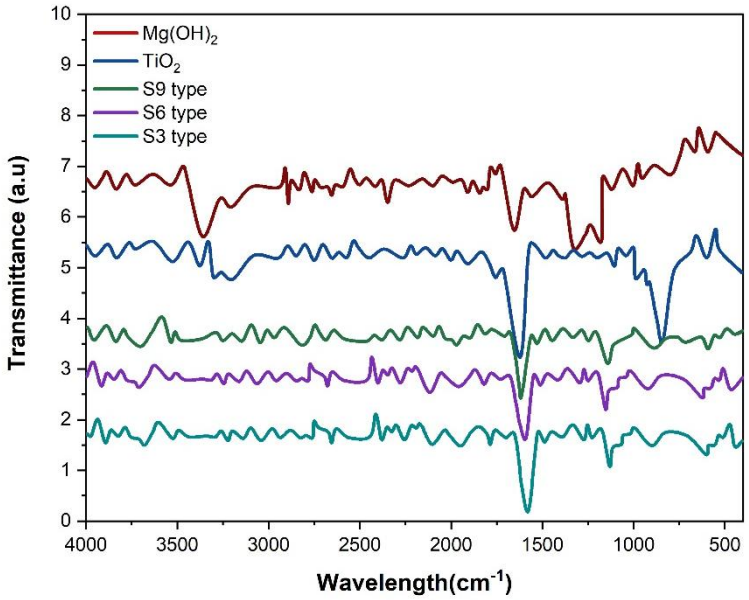

Figure 4. FTIR analysis of Prosopis juliflora/TiO_2/(Mg $(OH)_2$) hybrid composites.

The broad absorption band observed at 3200–3400 cm^{-1} corresponds to O–H stretching vibrations of cellulose and absorbed moisture. The peak at ~2920 cm^{-1} is attributed to C–H stretching of aliphatic groups.

The absorption near 1730–1745 cm^{-1} represents C=O stretching of hemicellulose. Conversely, this peak is absent in treated Prosopis juliflora fibers, indicating that the surface constituents have been either partially or completely eliminated from the fiber surfaces through hydroxide treatment. The carbonyl groups of hemicellulose are represented by an intensity peak at 2928 cm^{-1} in raw Prosopis juliflora fiber. The absence of this peak in treated Prosopis juliflora fiber indicates that the previously mentioned chemical treatments successfully eliminated the outermost layer of hemicellulose from the fiber. The band around 1600–1650 cm^{-1} corresponds to aromatic C=C stretching of lignin. Conversely, in chemically modified fiber, the peak shifts to 1648 cm^{-1}, showing that the lignin was entirely removed by the hydroxide treatment. The peak at ~1030–1150 cm^{-1} is associated with C–O–C stretching of cellulose. The maximum point for unprocessed fiber is noted at 1151 cm^{-1}. Conversely, for treated fiber, the maximum moves to 1157 cm^{-1} as a result of the cellulose absorption peak. The C–O and O–H stretching vibrations of the cellulose polysaccharide result in the peak at 1026 cm^{-1}. The peak at 814 cm^{-1} is attributed to the out-of-plane stretching of C–OH.

A comparison was conducted between the FTIR absorption and emission spectra of S3, S6, and S9-type materials and pure Prosopis juliflora composites. S3, S6, and S9 were used to illustrate epoxy/Prosopis juliflora hybrids in which titanium dioxide (TiO_2), magnesium hydroxide ($Mg(OH)_2$), or a combination of both was incorporated. These materials were selected for FTIR investigation due to the incorporation of both hybrid and individual fine particles. The spectra of S3, S6, and S9 composite materials exhibited no novel trends or peak displacements. The outcome indicated a slight reduction in transmission percentage at the peak frequency of 3316 cm^{-1} in the spectra of the S3, S6, and S9 hybrid types. Nano ($Mg(OH)_2$), TiO_2, and other chemicals with extensive OH categories successfully interact with the OH cellulose linkages in Prosopis juliflora fiber. Nanoparticles of TiO_2, $Mg(OH)_2$, and Prosopis juliflora fiber can establish significant hydrogen bonds on their outermost layer due to these interactions. The S3, S6, and S9 samples also intensified at 1722 cm^{-1}, indicating C=O stretching, which differs from the pure Prosopis juliflora hybrids. Epoxy and Prosopis juliflora fiber both contain nanosized particles of magnesium hydroxide and titanium oxide, and the superior dispersion of these particles explains the bonding between the two components. The FTIR study demonstrated the chemical compatibility of $Mg(OH)_2$ and TiO_2 nanoparticles with Prosopis juliflora fibers, enhancing surface contact in polymers. Previous research has demonstrated that FTIR analysis confirmed the presence of lignocellulosic functional groups in the electrodes by identifying the characteristic stretching and vibrational modes of carbon (C), hydrogen (H), and oxygen (O)-containing bonds. The spectra verified the successful incorporation of lignocellulose fibers into the TiO_2-based composite, indicating the preservation of the organic matrix essential for flexible electrode fabrication [24].

3.3 Mechanical Properties

3.3.1 Tensile Strength

The tensile stress–strain curves of all compositions (S1–S10) are shown in Figure 5 and exhibit typical brittle-to-semi-ductile behavior characteristic of thermoset-based natural fiber composites.

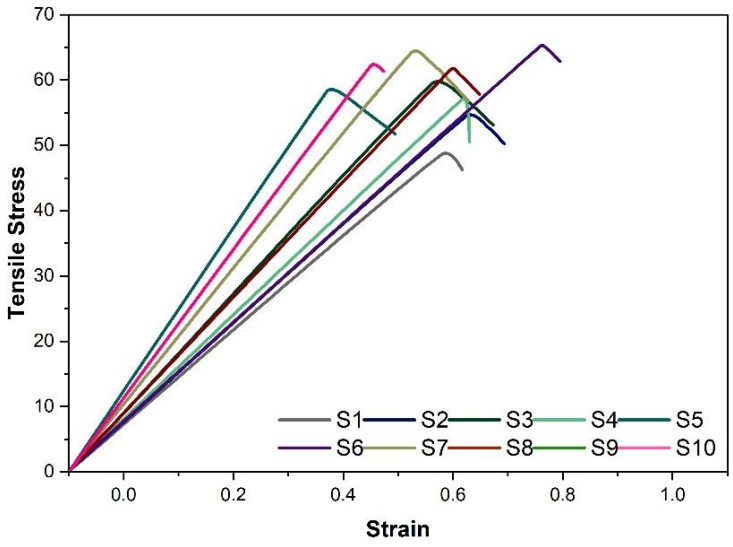

Figure 5. Evaluation of tensile stress-strain curves of the composites.

The control sample (S1) shows a comparatively lower slope in the elastic region and earlier fracture, indicating limited stress transfer between untreated fiber and epoxy matrix. The incorporation of $Mg(OH)_2$ nanoparticles (S2–S4) progressively increases tensile stiffness up to 4 wt.% (S3), where the maximum tensile strength of 59.38 MPa is observed. This improvement is attributed to uniform nanoparticle dispersion, enhanced interfacial bonding, and improved load transfer efficiency. However, at 6 wt.% (S4), the tensile slope slightly decreases, suggesting particle agglomeration and stress concentration zones. Similarly, TiO_2-filled composites (S5–S7) demonstrate enhanced tensile modulus and strength, with S6 (4 wt.% TiO_2) achieving the highest tensile strength of 64.60 MPa. The improved elastic slope indicates restricted polymer chain mobility and stronger fiber–matrix interaction due to high surface area nanoparticles. At 6 wt.% (S7), premature fracture and reduced elongation are observed, confirming nanoparticle clustering. Hybrid systems (S8–S10) exhibit balanced stiffness and ductility. Among them, S9 (3 wt.% $Mg(OH)_2$ + 1 wt.% TiO_2) demonstrates superior strain at failure and improved toughness due to synergistic interaction between both fillers. Overall, the optimum tensile performance at 4 wt.% loading is governed by uniform dispersion and efficient stress transfer, while excessive loading results in agglomeration-induced mechanical degradation.

Epoxy and Prosopis juliflora hybrid composites exhibited significant enhancements in tensile strength and modulus with the incorporation of Mg $(OH)_2$, TiO2, and both fillers (Figure 6). The use of 4 wt% Mg (OH)2 and TiO2 nanoparticles in epoxy/Prosopis juliflora hybrids yielded optimal results in terms of tensile strength and elongation. Polymers including a blend of Mg (OH)2 and TiO_2 particles at 4 wt.% were also examined and are illustrated in Figure 6. Various nanocomposite forms yielded a 19.76% enhancement (59.38 MPa), a 30.29% enhancement (64.60 MPa), and a 17.95% enhancement (58.48 MPa) in the tensile strength of the purified Prosopis juliflora composites (49.58 MPa), respectively. Because TiO2 possesses a higher number of OH groups than Mg (OH)2, its tensile properties surpass those of epoxy/Prosopis juliflora hybrids reinforced with Mg (OH)2. The improved tensile behavior of the hybrids results from the uniformly dispersed nanoparticles in the synthetic resins and the robust interfacial interactions between the Prosopis juliflora fibers and the nanoparticles, as evidenced by FTIR analyses. Similarly, the incorporation of CuO and TiO_2 microparticles considerably improved the mechanical performance of jute/JUCO/glass hybrid epoxy composites. The 3 wt.% CuO composites exhibited the highest tensile strength (63.68% improvement), indicating enhanced load-transfer efficiency and stronger interfacial adhesion between the fibers, matrix, and filler particles [25].

As the nanoparticle concentration exceeded 4 wt%, the tensile strength of the materials diminished. Particles tend to aggregate, and nanomaterials exhibit poor dispersion within matrices when present in large quantities because of the predominance of van der Waals forces in the interactions among individual particles. The epoxy/Prosopis juliflora composite exhibited an enhancement in its elastic modulus following the inclusion of nanomaterials.

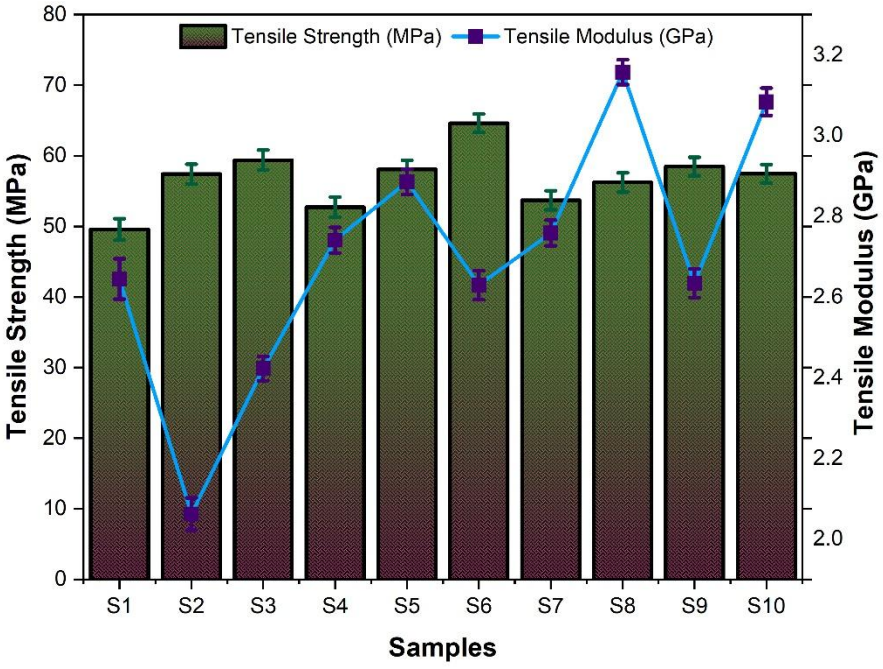

Figure 6. Tensile strength and modulus of Prosopis juliflora fibers/ TiO_2/(Mg $(OH)_2$)- hybrid composites.

Untreated fiber composites had much lower tensile strength than those treated with hydroxide. The XRD analysis indicates that the fibers exhibit increased crystallinity post-treatment, which is a principal rationale for this enhancement. As crystallinity increases, cellulose chains exhibit greater rigidity, facilitating the transfer of stresses from the fiber to the matrix. The hydroxide treatment enhances physical and chemical integration with the polymer matrix by refining the fiber surface and eliminating the majority of non-cellulosic contaminants. The enhanced tensile strength of hybrid composites following hydroxide treatment is attributable to these structural features. Nanoparticles of titanium dioxide and magnesium hydroxide have demonstrated enhancements in modulus and tensile strength, consistent with current developments in advanced fiber composites. The decline in tensile strength at loadings above 4 wt% is attributed to particle agglomeration, consistent with nanoparticle saturation effects. In such instances, an excess of filler material led to the creation of stress concentration points, thereby undermining the mechanical integrity of the material. This aligns with the prevailing belief that nanoparticle dispersion and optimal loading significantly influence the tensile properties of biocomposites.

3.3.2 Flexural Strength

Figure 7 shows the flexural stress–strain curves of all samples under three-point bending, exhibiting linear elastic behavior followed by sudden fracture, which is typical of epoxy-based composites. The control specimen (S1) exhibits the lowest flexural stiffness and early crack initiation due to limited interfacial bonding.

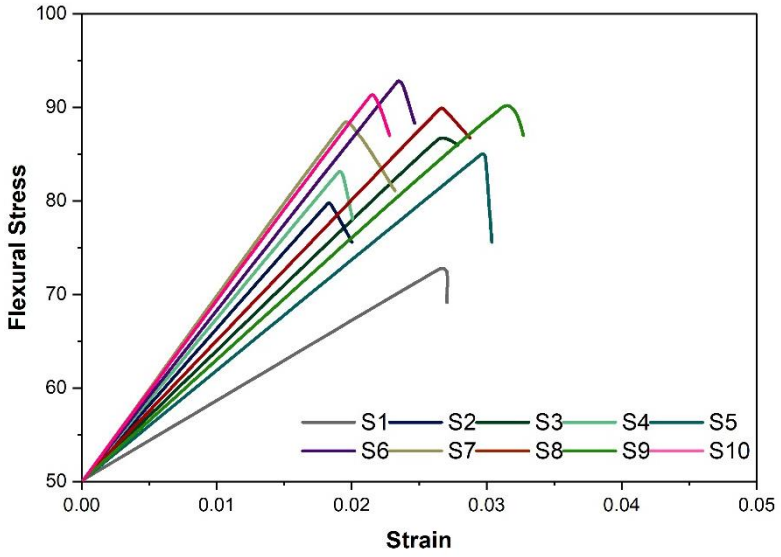

Figure 7. Evaluation of flexural stress-strain curves of the composites.

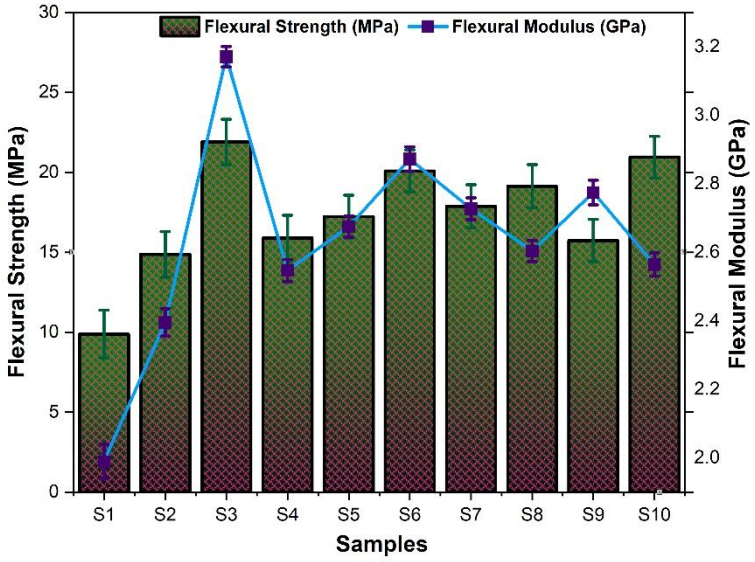

Figure 8. Flexural strength and modulus of Prosopis juliflora/TiO_2/($Mg(OH)_2$) hybrid composites.

With $Mg(OH)_2$ addition (S2–S4), flexural stiffness increases progressively, reaching optimum performance at S3 (4 wt.%), where improved matrix rigidity and crack resistance are observed. At 6 wt. % (S4), slight reduction in strain capacity indicates localized particle clustering affecting stress distribution. TiO_2-reinforced composites (S5–S7) display greater flexural modulus enhancement compared to $Mg(OH)_2$ systems, with S6 (4 wt.%) achieving significant bending resistance. The improved slope in the elastic region confirms effective nanoparticle reinforcement and reduced microcrack propagation. However, excessive TiO_2 content (S7) results in marginal stiffness reduction due to aggregation. Hybrid compositions (S8–S10) exhibit improved energy absorption under bending. S10 (2 wt.% $Mg(OH)_2$ + 2 wt.% TiO_2) shows balanced stiffness and ductility, attributed to synergistic dispersion effects and enhanced interfacial stress redistribution. The improved bending performance at optimized filler loading confirms that controlled nanoparticle incorporation enhances resistance to crack initiation and propagation, whereas higher loading induces microstructural heterogeneity and stress concentration.

Figure 8 illustrates the modulus and flexural strength of all the nanocomposites. The incorporation of nano (Mg $(OH)_2$) and TiO_2 into this epoxy/Prosopis juliflora hybrid enhanced its elasticity and flexural strength. The modulus and bending strength of the polymers improved for the same reasons as their tensile strength and modulus. The interaction of Mg $(OH)_2$ and TiO_2 with Prosopis juliflora fiber, along with finely dispersed nanomaterials in the epoxy matrix, improved the flexural capabilities of S1-type hybrids. Nanostructures enhance bending capabilities by restricting the mobility of polymer molecules, thereby facilitating their interactions. The results indicate that the S3, S6, and S10 composite types exhibit greater flexibility than the S1 composite type, with increases of 54.86% (21.89 MPa), 50.79% (20.08 MPa), and 52.81% (20.94 MPa) compared to the S1 composite type, respectively. The addition of nanoparticles into the S1-type composite improved its bending modulus. The maximum bending modulus for all hybrids was determined to be 2.54 GPa for S4-type, 2.72 GPa for S7-type, and 2.77 GPa for S9-type. In a previous study, the addition of 3 wt.% TiO_2 nanofiller markedly enhanced the mechanical properties of sisal/banana fiber hybrid epoxy composites. The optimized composite achieved a flexural strength of 94.86 MPa owing to improved interfacial bonding between the fibers and matrix [26].

This study demonstrated that hybrid composites containing Prosopis juliflora fibers, along with dispersed Mg $(OH)_2$ and TiO_2 nanoparticles, exhibited enhanced flexural properties because molecular slippage within the matrix was restricted. The notable enhancement in flexural strength, which has now attained 54%, substantiates the premise that the efficacy of bio-based composites in foundational structures can be improved. This indicates that mechanical performance is significantly enhanced with meticulously regulated nanoparticle integration.

3.3.3. Impact Strength

Figure 9 illustrates the impact resistance of the materials. The impact response exhibited patterns analogous to those of bending and tensile strength with the incorporation of each distinct nanoparticle. Filled polymers of the S3 and S6 composites showed an escalation in energy absorption capability with the addition of each particle. Nonetheless, the hybrid material featuring the multi-particle packing of S9 composites exhibited the most remarkable impact performance relative to all others.

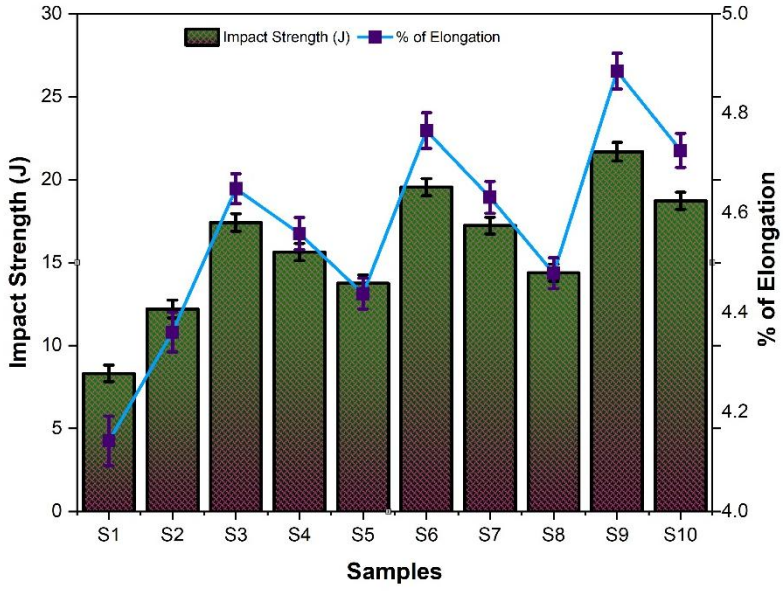

Figure 9. Impact strength of Prosopis juliflora/TiO_2/(Mg $(OH)_2$) with different mass proportions of nanofillers.

The findings indicate that the amalgamation of Mg $(OH)_2$ and TiO_2 nanoparticles enhances the efficacy of epoxy and Prosopis juliflora composites in moderating impact properties. The energy necessary to fracture particle-filled hybrids exceeds that of single-particle-based hybrids because the friction coefficient ratio between different nanomaterials is greater than that of solitary nanomaterials. Hybrid materials exhibiting improved impact characteristics are comparable to the concept of nanoparticles functioning synergistically. Composite materials S3, S6, and S9 have superior energy absorption capabilities compared to type S1 (8.32 kJ/m^2), with enhancements of 45.5% (17.41 kJ/m^2), 63.6% (19.74 kJ/m^2), and 71.2% (21.67 kJ/m^2), respectively. Several researchers have reported that the incorporation of B_4C and TiO_2 fillers significantly improved the mechanical performance of Canna indica/curaua fiber-reinforced hybrid composites. The composite containing 3 wt% TiO_2 exhibited the highest impact strength (10.7 J/m²), while both fillers enhanced tensile strength and reduced surface defects through improved fiber–matrix adhesion [27].

Enhanced particle dispersion and robust interfacial adhesion inhibited fracture development under dynamic loading, thereby augmenting toughness. This research showed that the addition of TiO_2 and Mg $(OH)_2$ as dual reinforcements augmented the energy necessary for crack initiation and propagation, attributable to their distinct surface characteristics, mechanisms, and energy absorption frameworks. It aligns with the finding that hybrid nanoparticles enhance impact resistance in biocomposite systems by deforming the matrix due to augmented interfacial friction.

3.3.4 SEM Analysis

Figure 10 presents SEM micrographs of untreated and hydroxide-treated *Prosopis juliflora* fibers. In the untreated fiber (Figure 10a), the surface appears relatively smooth, with the presence of impurities, waxy substances, and residual lignin covering the fiber bundles. These surface deposits hinder proper interfacial adhesion with the polymer matrix. In contrast, the hydroxide-treated fiber (Figure 10b) shows a comparatively rougher morphology with the removal of hemicellulose, surface wax, and amorphous components. The increased surface roughness and exposure of fibrillar structures facilitate enhanced mechanical interlocking with the matrix, thereby improving the fiber–matrix bonding potential.

The fracture behavior of epoxy/Prosopis juliflora fiber composites was examined by SEM of the tensile-cracked surfaces, as illustrated in Figure 11, to assess the influence of $Mg(OH)_2$ and TiO_2 nanoparticles. Figure 11a illustrates the untreated S1-type hybrid exhibiting pronounced fiber–matrix debonding and void formation, signifying inadequate adhesion and suboptimal stress transfer. Figure 11b illustrates fiber pull-out and interfacial voids, thereby corroborating inadequate bonding in the absence of nanoparticles. Conversely, Figure 11c illustrates fiber bundles more effectively integrated within the matrix, indicating that the incorporation of 4 wt.% TiO_2 nanoparticles markedly improved fiber–matrix interlocking and stress transfer. This enhancement is due to the synergistic actions of the nanofillers, wherein hydrogen bonding between cellulose hydroxyl groups and nanoparticle surfaces fortifies adhesion. The non-monotonic trend observed in tensile modulus with increasing TiO_2 loading is attributed to nanoparticle dispersion behavior. At 4 wt.%, uniform dispersion enhances stress transfer efficiency; however, at 6 wt.%, particle agglomeration leads to stress concentration zones, as confirmed by SEM micrographs showing clustered particles. Similar behavior has been reported in nanoparticle-reinforced epoxy composites where excessive filler loading reduces effective reinforcement efficiency [11].

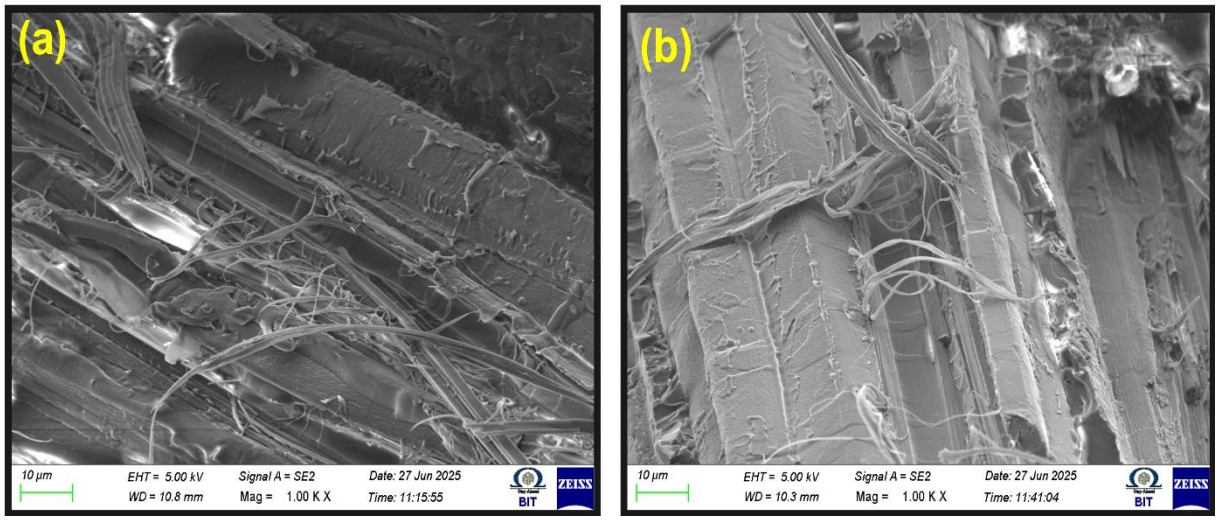

Figure 10. SEM micrographs of **(a)** untreated and **(b)** hydroxide-treated Prosopis juliflora fiber.

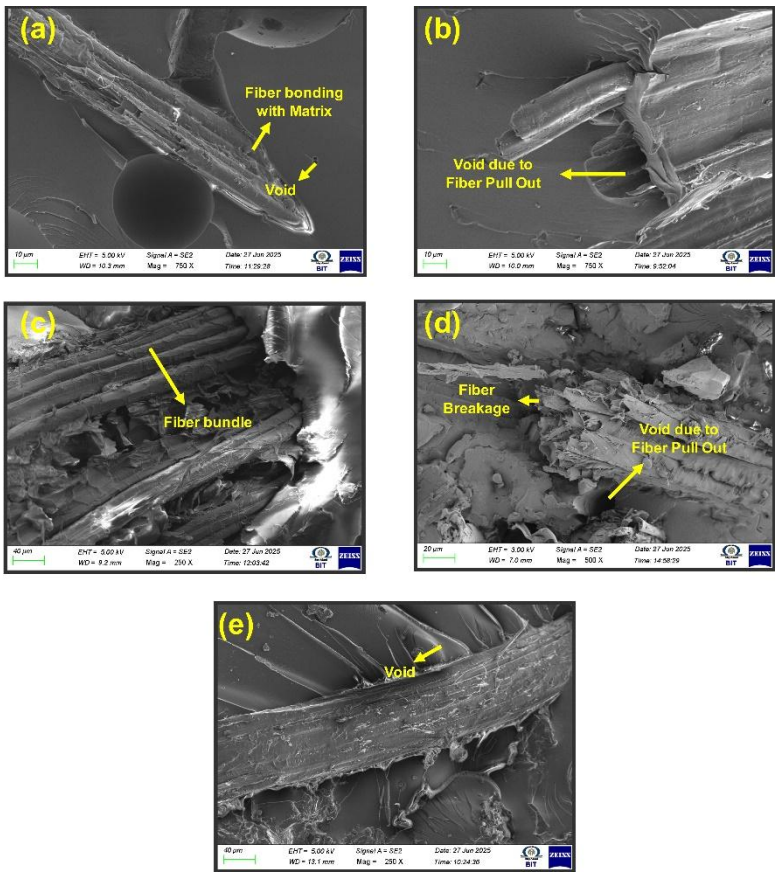

Figure 11. SEM of **(a)** Pure Prosopis juliflora fiber **(b)** 4 wt.% of (Mg $(OH)_2$) **(c)** 4 wt.% of TiO_2 **(d)** 6 wt.% of (Mg $(OH)_2$) and **(e)** 6 wt.% of TiO_2 filled hybrid composites**.**

Figures 11d and 11e demonstrate the emergence of voids and fiber fracture, accompanied by localized particle agglomerations, especially at elevated filler loadings. These agglomerates arise from excessive integration of nanoparticles, which promotes particle–particle interactions at the expense of particle–fiber bonding, resulting in stress concentration points and localized failures. This tendency has been extensively documented in nanofilled composites, where high filler content reduces effective dispersion. The SEM data corroborate the tensile test results, indicating that a moderate addition of nanoparticles enhances fiber-matrix adhesion and fracture resistance, but excessive loading leads to clustering and diminishes reinforcement efficacy.

3.4 Flammability Characteristics

3.4.1 Burning Experiment

A horizontal combustion experiment was performed on both nanomaterial-infused and non-nanomaterial materials. Figure 12 illustrates several flammability characteristics, including combustion duration and velocity. The addition of TiO_2 and Mg $(OH)_2$ to the composite materials prolonged their burning duration and reduced their combustion rate. This may be attributed to the diminished gaseous phase, the insulating properties of dissolved magnesium oxide and titanium oxide coatings against heat and mass transfer, and the presence of water vapor at the material interfaces, all of which contribute to this phenomenon. The combustion durations of composites S4, S7, and S10 increased by 75% (30.5 s), 87.5% (35.2 s), and 95% (42.3 s), respectively, in comparison to the S1-type hybrid (14 s). No reference to the combustion grade was made; nonetheless, the burn rates for S1-type and S5-type materials were 70 mm/min and 55 mm/min, respectively, both surpassing 35 mm/min. All other materials had combustion indices below 35 mm/min. A previous study reported that the incorporation of magnesium hydroxide ($Mg(OH)_2$) significantly enhanced the flammability resistance of kenaf fiber/PET-reinforced epoxy composites by reducing the horizontal burning rate. Among all formulations, the composite containing 35 wt% kenaf fiber (epoxy/PET/KF-35) exhibited the best flame-retardant performance, achieving the lowest average burning rate of 14.55 mm/min due to its improved composite integrity and fewer surface defects [13].

3.4.2 Cone Calorimeter Analysis

The combustion rate of the examined materials is indicated by the significant phenomenon referred to as DI. The DI of the S1-type composite was 14 seconds; however, it increased in all other hybrids due to the decomposition of Mg $(OH)_2$ and TiO_2 into water

molecules, facilitating the cooling and liquefaction of combustible gases. To assess the fire resistance of the composite material, RHL is the most critical factor to consider. Figure 13 displays the RHL contours of all the combined specimens. The S1-type laminate ignited rapidly at a peak intensity of 420 kW/m^2. The maximum heat release rate (HRHL) of the materials was markedly decreased following the incorporation of nanoparticles. In comparison to the highest rate of heat liberation of epoxy/Prosopis juliflora composites (420 kW/m²), the S4-type exhibited a loss of 4.3% (402 kW/m²), the S7-type a reduction of 2.1% (411 kW/m²), and the S10-type a decrease of 2.8% (408 kW/m^2). The capacity of nanoscale TiO_2 and Mg $(OH)_2$ particles to create charred areas, an accomplishment unattainable by either epoxy or Prosopis juliflora fiber composites, accounts for the reduction in the highest rate of heat liberation.

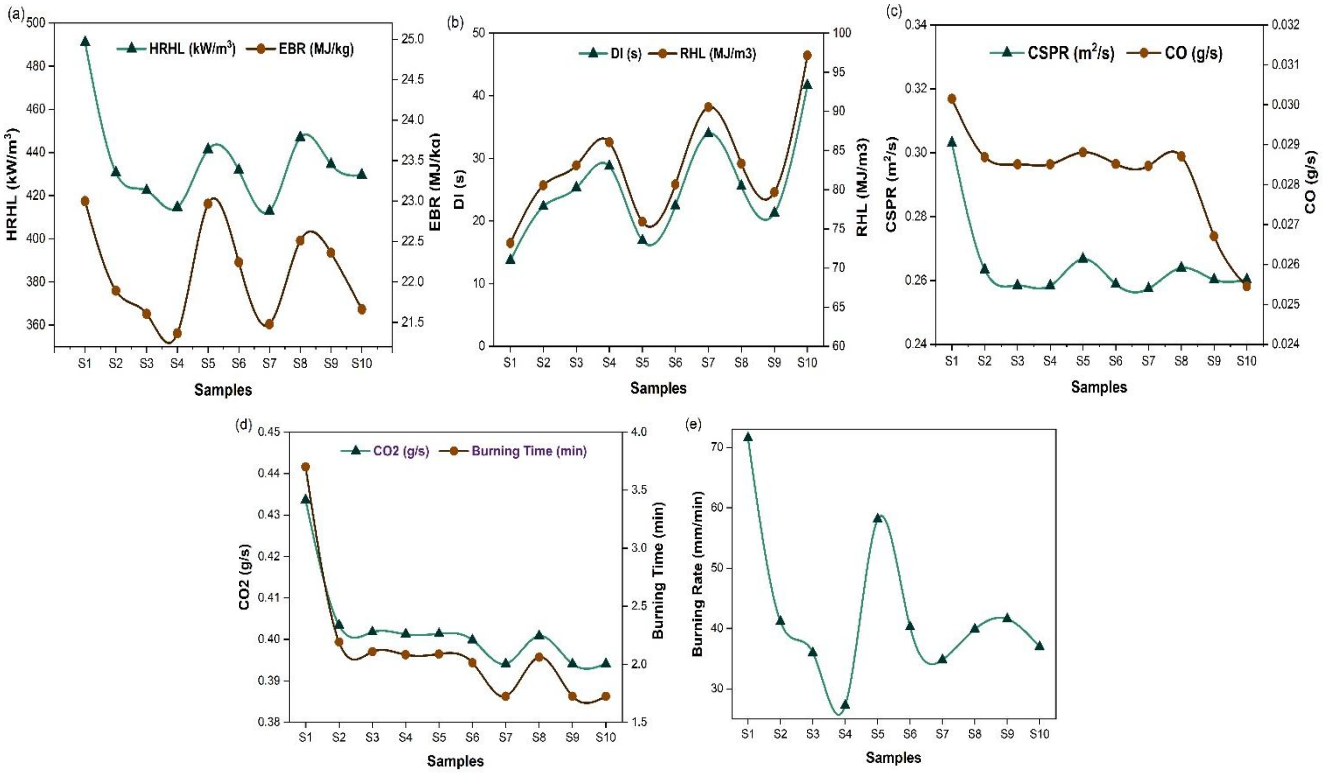

Figure 12. Flammability characteristics of **(a)** HRHL & EBR, **(b)** DI & RHL, **(c)** CSPR & CO, **(d)** CO_2 & burning time, **(e)** burning rate of TiO_2/(Mg $(OH)_2$)/Prosopis juliflora fiber-based hybrid composites.

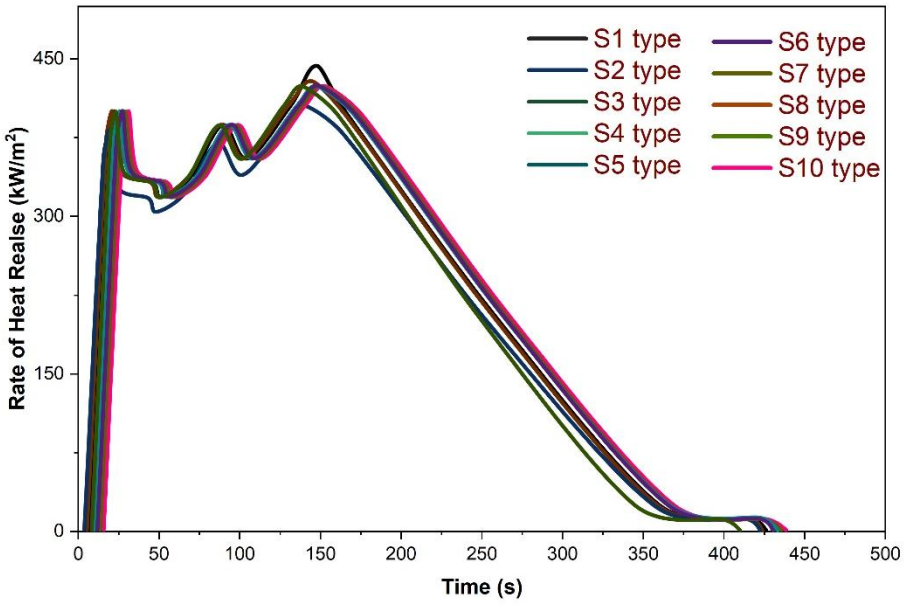

Figure 13. Heat release rate of various composites during combustion.

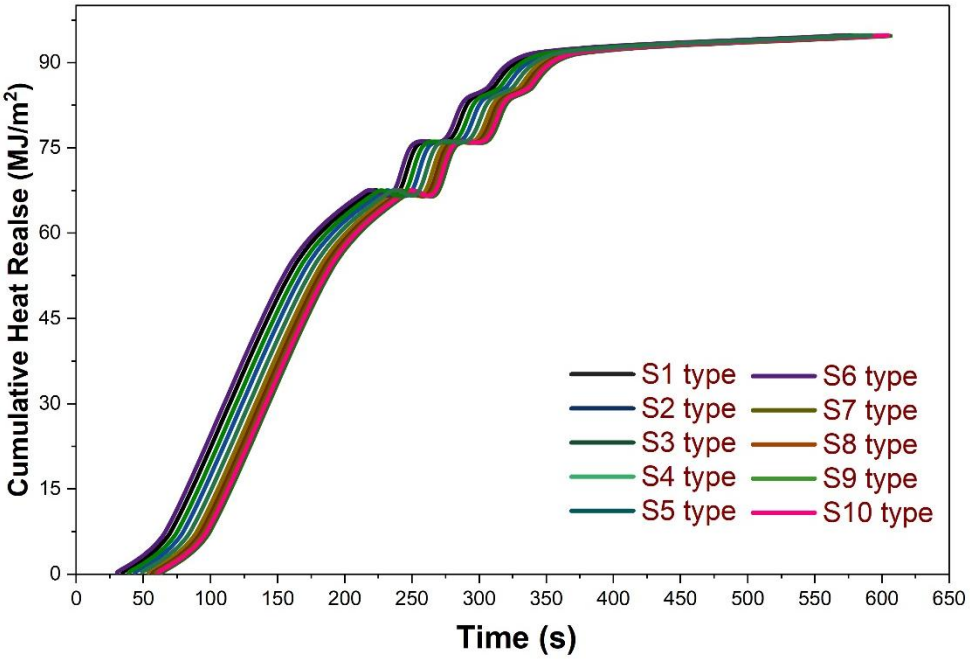

Figure 14. Cumulative heat release rate of various composites during combustion.

The formation of a char layer primarily diminishes HRHL, thereby enhancing fire-resistant characteristics. The amalgamation of $Mg(OH)_2$ and TiO_2 enhances the density of the char covering, thereby diminishing heat transfer and augmenting the fire resistance of epoxy/Prosopis juliflora hybrid composites.

Figure 14 shows the RHL for each composite. The incorporation of tiny particles greatly reduced the RHL of the nanocomposite. The S4-type RHL decreased by 4.2% (92 MJ/m^2), the S7-type RHL decreased by 3.1% (93 MJ/m^2), and the S10-type RHL decreased by 2.1% (94 MJ/m^2) relative to the S1-type combination's RHL (96 MJ/m^2). The combustion of Mg $(OH)_2$ and TiO_2 particles resulted in the formation of an oxide layer, which decreased CHL readings and functioned as a char buffer. The generation rates of carbon dioxide (CO_2) and carbon monoxide (CO), along with the cumulative smoke production rate (CSPR), are significant factors in flame-suppression characteristics. Subsequent to the addition of Mg $(OH)_2$, TiO_2, or both, these variables exhibited a pattern comparable to that of RHL.

3.5 Thermal Degradation

An investigation into the thermal resistance of the polymers was conducted. Table 3 presents several pertinent parameters, whereas Figures 15 and 16 illustrate the TGA and DTG contours, respectively. The initial breakdown temperatures of hybrid composites increased with the addition of TiO_2 and Mg $(OH)_2$ nanoparticles. The S1, S7, and S10 hybrids exhibited onset temperatures of 348.6 °C, 342.8 °C, and 338.9 °C, respectively, exceeding the S1 hybrid's 325.4 °C.

Table 3 presents the maximum temperature (T_{max}), a significant temperature change, and the juncture at which mass loss is most apparent. The composite's maximum breakdown temperatures are indicated by two distinct peaks on the DTG chart, referred to as T_{max1} and T_{max2}. In the comparison of T_{max1} and T_{max2}, the latter exhibited a more significant weight loss. The augmentation of T_{max1} and T_{max2} in the S1-type composite following the incorporation of nanomaterials is evident. The endothermic decomposition of nanosized granules of Mg $(OH)_2$ and TiO_2 is undoubtedly responsible for this. The breakdown temperatures of titanium dioxide (TiO_2) and magnesium hydroxide (Mg $(OH)_2$) are 340 °C and 370 °C, respectively. At temperatures ranging from 330 to 380 °C, titanium dioxide (TiO_2) and magnesium hydroxide (Mg $(OH)_2$) decompose, releasing water vapor and resulting in the formation of a thin oxide layer on the surface of the composite material, which functions as an insulator. The reduced passage of heat and mass through the insulating material enhances temperature stability. The S10-type composite exhibits a second thermal degradation temperature peak (T_{max2}) that is 3.34% greater than that of the S1-type hybrid, while the S4-type composite demonstrates a relative rise of 5.08% and 4.42%. This demonstrates that epoxy/Prosopis juliflora fiber hybrids can achieve enhanced heat resilience through the incorporation of $Mg(OH)_2$, TiO_2, and their interaction. Nanoscale Mg $(OH)_2$ and TiO_2 fillers augmented the char deposition in S1-type hybrids, as illustrated in Figure 14 and Table 3. Charred deposits were measured at 11.54%, 10.76%, and 10.61% in the S4, S6, and S10 hybrids, respectively, in contrast to the S1 hybrid's 9%.

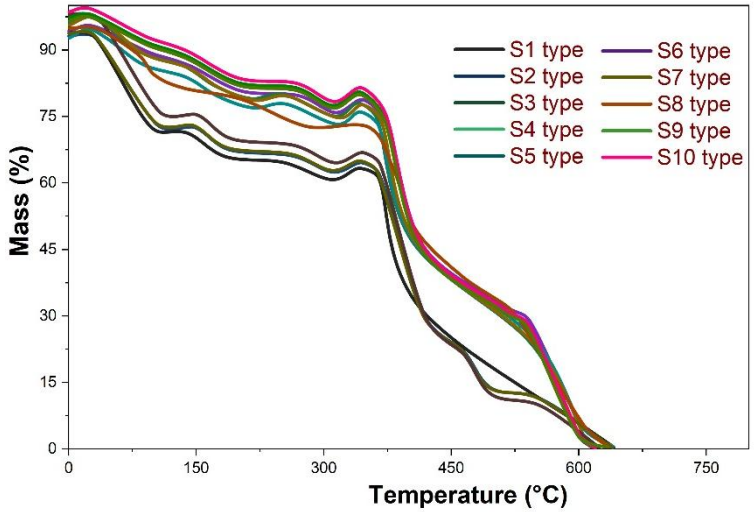

Figure 15. TGA curve of Prosopis juliflora fibers/ TiO_2/(Mg $(OH)_2$)- hybrid composites.

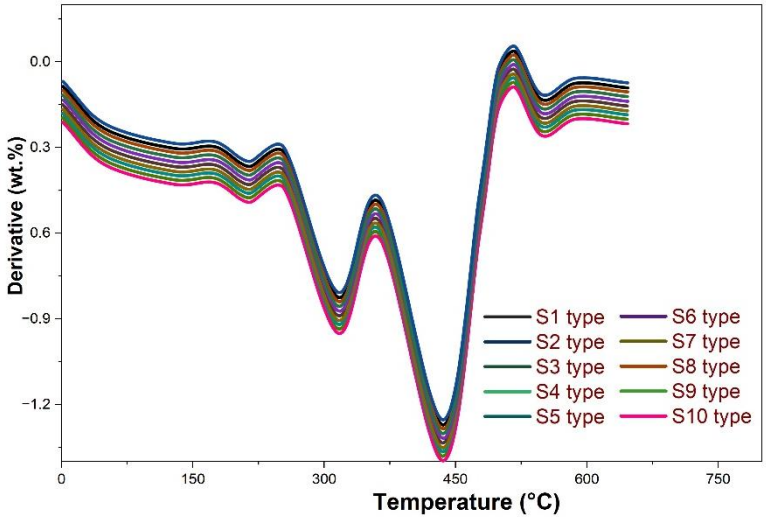

Figure 16. DTG curve of Prosopis juliflora fibers/ TiO_2/(Mg $(OH)_2$).

Table 3. Thermal decomposition of Prosopis juliflora fiber / TiO_2/(Mg $(OH)_2$)-based hybrid composites

Sl.No	Specimen	T_0(℃)	T_{max}(℃)		Char residue (%)
			T_{max1}(℃)	T_{max2}(℃)	
1	S1	325	384	430	9.9
2	S2	338	397	440	9.5
3	S3	340	398	442	9.6
4	S4	349	399	452	11.5
5	S5	342	396	439	9.0
6	S6	341	398	445	10.8
7	S7	343	401	449	10.4
8	S8	346	402	441	8.7
9	S9	344	395	436	8.5
10	S10	339	397	447	10.6

This phenomenon illustrates how S1-type polymers can be enhanced in thermal stability through the incorporation of nano-sized Mg $(OH)_2$, TiO_2, or a combination of both. Prior investigations have shown the thermal stability of flame-retardant natural fiber composites using thermogravimetric analysis (TGA) to assess their degradation behavior. The TGA results indicated that composites containing Mg(OH)2, zinc borate, and zirconium oxide exhibited superior thermal stability and enhanced resistance to thermal decomposition compared to the other flame-retardant formulations [28].

3.6 Water Absorption Analysis

Figure 17 presents a comparison of moisture absorption over 0 to 196 hours for both raw and hydroxide-treated materials. All investigated composites exhibited analogous water-resistance patterns, which is logical considering they were uniformly reinforced with 20 wt.% fiber packing. Both untreated and chemically treated composites demonstrated a significant increase in water absorption rate over a duration of up to 168 hours. The saturation of the composite samples results in a decrease in the fluid absorption rate for all composite specimens, which stabilizes after 168 hours. A multitude of studies corroborated conclusions similar to those of the present experiments. The hydroxide-treated samples exhibited superior water absorption resistance compared to the raw materials. The aggregates derived from processed Prosopis juliflora fibers appear to exhibit reduced water uptake as a result of the extraction of lignin and hemicellulose during chemical treatment. Hemicellulose present in Prosopis juliflora fiber exhibits greater permeability and water absorption capacity compared to crystalline cellulose. Chemical processing may have enhanced the water-repellent characteristics of chemically modified fiber hybrids by fortifying the link between the fiber and matrix.

Figure 18 illustrates the response of hybrid materials to moisture retention. The materials comprise processed Prosopis juliflora fiber in different weight ratios with (Mg (OH)$_2$) nanofillers. Nanosized TiO_2 and Mg (OH)$_2$ often diminish water absorption in Prosopis juliflora fiber composites in comparison to untreated composites. This phenomenon is attributable to the remarkable barrier characteristics of the nanofillers. The inclusion of Mg (OH)$_2$ and TiO_2 at considerable ratios may hinder the penetration of water molecules into the aggregates.

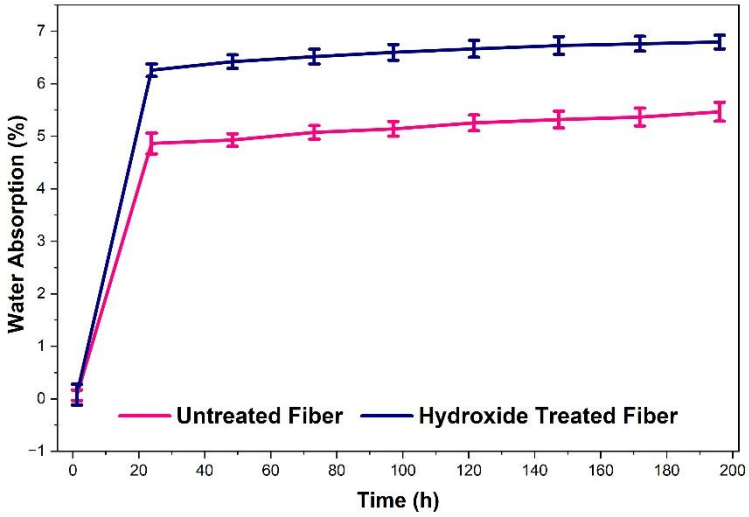

Figure 17. Water absorption characteristics of untreated and alkali-treated Prosopis juliflora fiber-based composites.

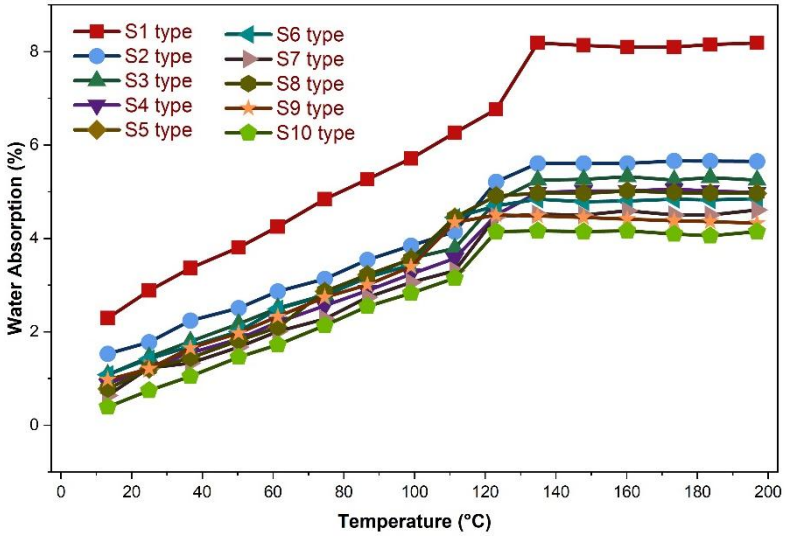

Figure 18. Water absorption behavior of Prosopis juliflora fiber/ TiO_2/(Mg (OH)$_2$)- hybrid composite.

Composites reinforced with Prosopis juliflora, nano-(Mg $(OH)_2$), and TiO_2 demonstrate a reduction in maximum water absorption as additive loading increases. The use of Prosopis juliflora fiber in epoxy composites results in enhanced water absorption. In comparison to pure epoxy with Prosopis juliflora fiber, Prosopis juliflora fiber/epoxy hybrids filled with nano (Mg $(OH)_2$) and TiO_2 at 2, 4, and 6 wt.% fillers, respectively, decrease maximum water absorption by 8.18%, 5.60%, and 5.24%. Water absorption has been reduced due to the escalating quantity of filler in all mixtures. Luffa/epoxy composites with 5 wt% TiO_2 nanoparticles showed tensile, flexural, and impact strengths improved by 74%, 54%, and 42%, respectively, while water absorption decreased by 98% [29].

4. Conclusion

The study demonstrated that incorporating $Mg(OH)_2$ and TiO_2 nanofillers significantly enhanced the structural, thermal, and fire-retardant performance of epoxy/*Prosopis juliflora* fiber composites. These findings confirm that $Mg(OH)_2$ and TiO_2 nanofillers significantly enhance the structural, thermal, and fire-retardant performance of epoxy/*Prosopis juliflora* fiber composites. XRD analysis revealed an increase in crystallinity index from 71.86% to 72.98% after alkali treatment, indicating effective removal of amorphous constituents and improved cellulose ordering. FTIR spectra confirmed enhanced interfacial compatibility through strengthened O–H interactions between nanofillers and cellulose. SEM micrographs showed uniform nanoparticle dispersion and improved fiber–matrix adhesion at 4 wt.% loading, while 6 wt.% resulted in agglomeration and localized stress concentration. The optimum 4 wt.% composition achieved maximum tensile strength (64.60 MPa), flexural strength (21.89 MPa), and impact strength (21.67 kJ m^{-2}), corresponding to improvements of 30.29%, 54.86%, and 71.2%, respectively, compared to the control. Thermal analysis demonstrated increased onset degradation temperature up to 348.6 °C and higher char residue (11.5%), while cone calorimetry showed reduced peak heat release rate from 420 to 402 kW m^{-2} and improved burning resistance below 35 mm min^{-1}. Water absorption decreased by 8.18% due to enhanced barrier properties. Future research may explore advanced nanoparticle dispersion techniques, hybrid filler optimization, fatigue and long-term durability studies, and life-cycle sustainability assessment to expand structural and fire-resistant applications.

References

[1] P. Madhu, M.R. Sanjay, A. Khan, A.A. Otaibi, S.A. Al-Zahrani, S. Pradeep, B. Yogesha, P. Boonyasopon, S. Siengchin, Hybrid Effect of PJFs/E-glass/Carbon Fabric Reinforced Hybrid Epoxy Composites for Structural Applications. Journal of Natural Fibers, 19(10), (2022) 3742-3752. https://doi.org/10.1080/15440478.2020.1848724

[2] G.S. Balan, V. Kumar, M. Ravichandran, Study of Ageing Effect on Mechanical Properties of Prosopis Juliflora Fibre Reinforced Palm Seed Powder Filled Polymer Composite. Australian Journal of Mechanical Engineering, 20(5), (2022) 1413-1425. https://doi.org/10.1080/14484846.2020.1806194

[3] R. Thandavamoorthy, V. Mohanavel, A. Sivapragasam, V. Vekariya, D. Paul, P. Velmurugan, S. Al Obaid, S.A. Alharbi, N. Basavegowda, Environmental Sustainability and Waste Conversion of Prosopis Juliflora Fibre-Reinforced ZnO Nanofiller Particulates PLA Composite-Mechanical and Thermal Analysis. Heliyon, 10(19), (2024) e38327 https://doi.org/10.1016/j.heliyon.2024.e38327

[4] J. Maniraj, F. Sahayaraj, J. Giri, T. Sathish, M.R. Shaik, Enhancing Performance of Prosopis Juliflora Fiber Reinforced Epoxy Composites with Silane Treatment and Syzygium Cumini Filler. Journal of Materials Research and Technology, 31, (2024) 93-108. https://doi.org/10.1016/j.jmrt.2024.06.058

[5] P.V. Reddy, R.V.S. Reddy, P. Rajendra Prasad, D. Mohana Krishnudu, R.M. Reddy, H.R. Rao, Evaluation of Mechanical and Wear Performances of Natural Fiber Reinforced Epoxy Composites. Journal of Natural Fibers, 19(6), (2022) 2218-2231. https://doi.org/10.1080/15440478.2020.1807441

[6] P. Madhu, S. Mavinkere Rangappa, A. Khan, A. Al Otaibi, S.A. Al-Zahrani, S. Pradeep, M.K. Gupta, P. Boonyasopon, S. Siengchin, Experimental Investigation on the Mechanical and Morphological Behavior of Prosopis Juliflora Bark Fibers/E-glass/Carbon Fabrics Reinforced Hybrid Polymeric Composites for Structural Applications. Polymer Composites, 41(12), (2020) 4983-4993. https://doi.org/10.1002/pc.25768

[7] S.K. Ramakrishnan, A. Arivendan, K. Vijayananth, Cellulose extraction from red sage fiber, Prosopis Juliflora fiber, Vegetable Waste Filler: Applications in PLA Based Bio Composites. International Journal of Biological Macromolecules, 285, (2025) 138102. https://doi.org/10.1016/j.ijbiomac.2024.138102

[8] N. Sakthieswaran, M. Sophia, Prosopis Juliflora Fibre Reinforced Green Building Plaster Materials -An Eco-Friendly Weed Control Technique by Effective Utilization. Environmental Technology and Innovation, 20, (2020) 101158. https://doi.org/10.1016/j.eti.2020.101158

[9] V. Ganesan, V. Shanmugam, V. Alagumalai, B. Kaliyamoorthy, O. Das, M. Misra, Optimisation of mechanical behaviour of Calotropis gigantea and Prosopis juliflora natural fibre-based hybrid

composites by using Taguchi-Grey relational analysis. Composites Part C: Open Access, 13, (2024) 100433. https://doi.org/10.1016/j.jcomc.2024.100433

[10] M.K. Gurunathan, N.R.J. Hynes, O.A. Al-Khashman, M. Brykov, N. Ganesh, A. Ene, Study on the Impact and Water Absorption Performance of Prosopis juliflora and Glass Fibre Reinforced Epoxy Composite Laminates. Polymers, 14(15), (2022) 2973. https://doi.org/10.3390/polym14152973

[11] K.R. Sumesh, G. Saikrishnan, P. Pandiyan, L. Prabhu, S. Gokulkumar, A.K. Priya, P. Spatenka, S. Krishna, The Influence of Different Parameters in Tribological Characteristics of Pineapple/Sisal/TiO_2 Filler Incorporation. Journal of Industrial Textiles, 51(5_suppl), (2022) 8626S-8644S. https://doi.org/10.1177/15280837211022614

[12] H.U. Zaman, R.A. Khan, Preparation and Testing of Bast Fiber Reinforced Thermoplastic Composites under Chemical Treatment. International Journal of Advanced Science and Engineering, 10(1), (2023) 3164-3177. https://doi.org/10.29294/IJASE.10.1.2023.3164-3177

[13] M.J. Suriani, H.A. Zainudin, R.A. Ilyas, M. Petru, S.M. Sapuan, C.M. Ruzaidi, R. Mustapha, Kenaf Fiber/Pet Yarn Reinforced Epoxy Hybrid Polymer Composites: Morphological, Tensile, and Flammability Properties. Polymers, 13(9), (2021) 1532. https://doi.org/10.3390/polym13091532

[14] B. Wu, J. Qiu, Incorporating Hollow Natural Fiber (HNF) to Enhance CO_2 Sequestration and Mechanical Properties of Reactive Magnesia Cement (RMC)-Based Composites: Feasibility study. Journal of CO_2 Utilization, 57, (2022) 101874. https://doi.org/10.1016/j.jcou.2021.101874

[15] P. Soni, S. Sinha, Fiber and Future: Unleashing the Power of Industrial Hemp Waste through Epoxy Composites. Polymer Composites, 45(1), (2024) 413-423. https://doi.org/10.1002/pc.27786

[16] T. Premkumar, N. Nagabhooshanam, P.S. Parihar, N. Bhosle, S. Supriya, V.S.N. Kumar, D. Barik, R. Srinivasan, S. Sathiyamurthy, Enrichment of Poly-Fiber Composites Functional Properties by the Influences of Hydrophobic Titanium Dioxide Nanoparticles Via Injection Mould Technique. Iranian Polymer Journal, 35(6), (2026) 1245-1259. https://doi.org/10.1007/s13726-025-01586-9

[17] S. Acharjya, S.P. Mohanty, Impact of Magnesium Hydroxide Particles Decorated Kenaf Fibre on the Physico-Mechanical Properties of Polypropylene-based Composites. Bulletin of Materials Science, 47(4), (2024) 275. https://doi.org/10.1007/s12034-024-03345-7

[18] A.B. Irez, Development of Sunflower Husk Reinforced Polypropylene based Sustainable Composites: An Experimental Investigation of Mechanical and Thermal Performance. Journal of Polymer Science, 62(15), (2024) 3471-3484. https://doi.org/10.1002/pol.20240162

[19] S.K. Mishra, A. Purohit, S. Palanimuthu, A. Kumar, Exploring the use of TiO_2 filler in short Ficus Benghalensis natural fibre-based polymeric composites. Plastics, Rubber and Composites, 54(3–4), (2025) 69–81. https://doi.org/10.1177/14658011251326451

[20] S.S. Kumar, P. Shyamala, P.R. Pati, J. Giri, E. Makki, T. Sathish, Mechanical (Static and dynamic) Characterization and Thermal Stability of Hybrid Green Composites for Engineering Applications. Journal of Materials Research and Technology, 30, (2024) 7214-7227. https://doi.org/10.1016/j.jmrt.2024.05.132

[21] C.R. Mahesha, R. Suprabha, M.S. Harne, S.G. Galme, S.G. Thorat, N. Nagabhooshanam, A.H. Seikh, M.H. Siddique, M. Markos, Nanotitanium Oxide Particles and Jute-Hemp Fiber Hybrid Composites: Evaluate the Mechanical, Water Absorptions, and Morphological Behaviors. Journal of Nanomaterials, 2022(1), (2022) 3057293. https://doi.org/10.1155/2022/3057293

[22] P. Madhu, M.R. Sanjay, P. Senthamaraikannan, S. Pradeep, S. Siengchin, M. Jawaid, M. Kathiresan, Effect of Various Chemical Treatments of Prosopis Juliflora Fibers as Composite Reinforcement: Physicochemical, Thermal, Mechanical, and Morphological Properties. Journal of Natural Fibers, 17(6), (2020) 833-844. https://doi.org/10.1080/15440478.2018.1534191

[23] P.V Reddy, R.V.S. Reddy, B.V Reddy, D.M. Krishnudu, P.R. Prasad, P.S. Rao, Enhancement of the Dynamic Mechanical and Dielectric Properties of Prosopis Juliflora Fiber-Reinforced Composites by Fiber Modification. Journal of Natural Fibers, 19(13), (2022) 6780-6796. https://doi.org/10.1080/15440478.2021.1932676

[24] S. Ilyas, I. Sultana, R. Nasar, I. Hanif, S.H.M. Jafri, M. Naveed-Ul-Haq, A. Razaq, Tuning of Electrical Conduction Properties of Natural Fibers and TiO_2 based Flexible Paper Composite Sheets by Electrodeposition of Metallic Nanolayers. Ceramics International, 47(20), (2021) 29435-29442.

[25] N. Sur, T. Nath, I.I. Zahid, A.K. Debnath, M.A. Hasib, D. Roy, Enhancing Mechanical and Physical Properties of Jute/JUCO/Glass Fiber Hybrid Composites Through TiO_2 and CuO Microparticle Reinforcement. SPE Polymers, 7(3), (2026) e70052. https://doi.org/10.1002/pls2.70052

[26] A. Kuppuraj, B.S. Sounthararajan, K. Ramaswamy, Effect of TiO_2 Nanoparticle

Reinforcement on the Mechanical and Tribological Performance of Natural Fiber Hybrid Polymer Composites. Polymers and Polymer Composites, 34, (2026) 09673911261455225. https://doi.org/10.1177/09673911261455225

[27] E. Subbarao, D. Sharma, P. Singh, R.K. Gupta, B. Gayathri, S. Mayakannan, Influence of B_4C and TiO_2 Fillers on Mechanical and Tribological Performance of Canna Indica/Curaua Fiber Reinforced Hybrid Composites with ANN Prediction. Interactions, 247(1), (2026)148. https://doi.org/10.1007/s10751-026-02511-z

[28] D. Sampathkumar, A. Mohankumar, A. Kulandaivel, V. Packkirisamy, Experimental Investigation on the Micro Structural and Flame Retardant Properties of Various Natural Fiber Reinforced Composites. Journal of Natural Fibers, 21(1), (2024) 2341125. https://doi.org/10.1080/15440478.2024.2341125

[29] K. Anbukarasi, D. Mala, N. Senthilkumar, S.I. Hussain, S. Kalaiselvam, Investigation of TiO_2 Nanoparticles Influence on Tensile Properties and Thermal Stability of Dry and Wet Luffa-Epoxy Nanocomposites. Recent Patents on Nanotechnology, 19(4), (2025) 525-534. https://doi.org/10.2174/0118722105295445240418064351

Authors Contribution Statement

N. Shalom: Conceptualization, Investigation. R. Haridass: Data curation, Formal analysis, Resources. Pravin Kulurkar: Writing Review - Editing. S. Mayakannan: Methodology, Writing Original -Draft, Validation. All authors contributed to drafting and revising the manuscript.

Funding

The authors declare that no funds, grants or any other support were received during the preparation of this manuscript.

Competing Interests

The authors declare that there are no conflicts of interest regarding the publication of this manuscript.

Data Availability

The data supporting the findings of this study can be obtained from the corresponding author upon reasonable request.

Has this article screened for similarity?

Yes